Elsevier Editorial System(tm) for Remote Sensing of Environment
Manuscript Draft

Manuscript Number: RSE-D-11-00453

Title: Effective Tree Scattering and Opacity at L-Band

Article Type: Full length article

Keywords: radiometry; emission; opacity; albedo; scattering; L-band; forest; soil

Corresponding Author: Dr. Mehmet Kurum, Ph.D.

Corresponding Author's Institution: NASA GSFC

First Author: Mehmet Kurum, Ph.D.

Order of Authors: Mehmet Kurum, Ph.D.; Peggy E O'Neill; Roger H Lang, PhD; Alicia T Joseph, PhD; Michael H Cosh, PhD; Thomas J Jackson, PhD

Research highlights:

- Assessing applicability of the tau-omega model for tree canopies.
- Determining effective values for tau and omega for conifer trees.
- Relating the effective parameters to their theoretical definitions.

Effective Tree Scattering and Opacity at L-Band*

Mehmet Kurum[a], *Member, IEEE*, Peggy E. O'Neill[a], *Senior Member, IEEE*, Roger H. Lang[b], *Fellow, IEEE*, Alicia T. Joseph[a], Michael H. Cosh[c], and Thomas J. Jackson[c], *Fellow, IEEE*

[a] Hydrological Sciences Branch / Code 614.3 NASA Goddard Space Flight Center, Greenbelt, MD 20771 USA, Email: mehmet.kurum@nasa.gov , Tel: (301)614-6537, Fax: (301)614-5808

[b] Department of Electrical & Computer Engineering, George Washington University, Washington, DC 20052 USA

[c] Hydrology & Remote Sensing Laboratory, USDA ARS, Beltsville, MD 20705 USA

Abstract: This paper investigates vegetation effects at L-band by using a first-order radiative transfer (RT) model and truck-based microwave measurements over natural conifer stands to assess the applicability of the $\tau - \omega$ (tau-omega) model over trees. The tau-omega model is a zero-order RT solution that accounts for vegetation effects with effective vegetation parameters (vegetation opacity and single-scattering albedo), which represent the canopy as a whole. This approach inherently ignores multiple-scattering effects and, therefore, has a limited validity depending on the level of scattering within the canopy. The fact that the scattering from large forest components such as branches and trunks is significant at L-band requires that zero-order vegetation parameters be evaluated (compared) along with their theoretical definitions to provide a better understanding of these parameters in the retrieval algorithms as applied to trees. This paper compares the effective vegetation opacities, computed from multi-angular pine tree brightness temperature data, against the results of two independent approaches that provide theoretical and measured optical depths. These two techniques are based on forward scattering theory and radar corner reflector measurements, respectively. The results indicate that the

* This research was supported by an appointment to the NASA Postdoctoral Program at the Goddard Space Flight Center administered by Oak Ridge Associated Universities through a contract with NASA.

effective vegetation opacity values are smaller than but of similar magnitude to both radar and theoretical estimates. The effective opacity of the zero-order model is thus set equal to the theoretical opacity and an explicit expression for the effective albedo is then obtained from the zero- and first- order RT model comparison. The resultant albedo is found to have a similar magnitude as the effective albedo value obtained from brightness temperature measurements. However, it is less than half of that estimated using the theoretical calculations (0.5 – 0.6 for tree canopies at L-band). This lower observed albedo balances the scattering darkening effect of the large theoretical albedo with a first-order multiple-scattering contribution. The retrieved effective albedo is different from theoretical definitions and not the albedo of single forest elements anymore, but it becomes a global parameter, which depends on all the processes taking place within the canopy, including multiple-scattering.

1 INTRODUCTION

Soil moisture (SM) state is a key variable of the terrestrial water cycle. Global SM observations are of value in applications involving land-atmosphere interaction studies such as climate prediction, weather forecasting, water management, agricultural productivity estimation, and flood and drought hazards monitoring (Entekhabi et al., 1999). Microwave radiometry at low frequencies, such as L-band (1–2 GHz), has a great potential to sense to surface SM even if the soil is covered with vegetation. Several microwave space missions, such as ESA's Soil Moisture Ocean Salinity (SMOS) mission and NASA's Soil Moisture Active Passive (SMAP) mission (to be launched 2014), include an L-band radiometer and aim to provide the global measurements of the Earth's surface SM with an accuracy of 0.04 cm^3. cm^{-3} for those areas of the Earth's land

surface where vegetation water content (VWC) does not exceed 5 $kg.m^{-2}$ (Kerr et al., 2010; Entekhabi et al., 2010).

For routine SM retrievals over vegetated terrain, the spaceborne baseline algorithms use the tau-omega model (Mo, et al., 1982), a zero-order Radiative Transfer (RT) solution, due to its simplicity, and ease of inversion and implementation (Jackson, 1993; Owe et al., 2001; Njoku et al., 2003; Wigneron et al., 2007). This model links terrain geophysical variables to the observed brightness temperature through ground reflectivity and two vegetation parameters, the optical depth or opacity τ, and the single-scattering albedo ω. It has extensive heritage and has been effectively used in SM field campaigns (Jackson, 1993; Wigneron et al., 1995; Jackson et al., 1999) that cover grasslands, agricultural crops, and generally light to moderate vegetation. Forested areas have commonly been excluded from operational SM retrieval plans. There is some experimental and modeling evidence that microwave radiometry could be able to resolve the changes for some forest types in SM state (Lang et al., 2001; Della Vecchia et al., 2006;, Santi et al., 2009; Kurum et al., in press). However, sensitivity to SM is degraded significantly and the microwave forest emission is relatively invariable to the state of both SM and VWC (Grant et al., 2007; Della Vecchia et al. 2007; Guglielmetti et al., 2008; Grant et al., 2009; Kurum et al., submitted for publication) due to the large masking of trees on the microwave response to the underlying SM and/or the obscuring effect of the litter and understory layers. Knowledge of vegetation features at L-band appears to be of great importance for either correcting for the vegetation effects on SM retrievals or determining vegetation wet biomass itself. This paper is concerned with vegetation parameterization of the tau-omega model when applied over trees.

71 The tau-omega model loses its validity when there is dense vegetation (i.e. forest, mature corn,
72 etc.) with scatterers, such as branches and trunks (or stalks in the case of corn), which are large
73 with respect to the wavelength. More scattering terms (at least up to a first-order at L-band)
74 should be included in the RT solutions for forest canopies if these are expected to be accurate. A
75 recent study by Kurum et al., in press, proposed an additional first-order multiple-scattering term
76 to the tau-omega model to correct for large tree scattering. This additional term represents
77 emission by particles in the vegetation layer and emission by the ground that is scattered once by
78 particles in the layer. The resulting model represents an improvement over the standard zero-
79 order solution since it accounts for the scattered vegetation and ground radiation that can have a
80 pronounced effect on the observed emissivity and subsequent SM retrieval. On the other hand, a
81 zero-order approach might be still applied to vegetation canopies with large scatterers, using
82 equivalent or effective vegetation parameters (Ferrazolli et al., 2002). This approach requires
83 that the effective vegetation values (vegetation opacity and single-scattering albedo) be evaluated
84 (compared) with theoretical definitions of these parameters for forest canopies. The purpose of
85 this paper is to assess the applicability of the tau-omega model for tree canopies recognizing that
86 there is increased scatter from trees as compared to grasses and crops, and to determine the
87 effective values for tau and omega for trees and how these parameters are related to their
88 theoretical definitions.
89
90 Only a limited number of theoretical and experimental studies have addressed the topic of
91 effective tree parameterization (Ferrazolli et al., 2002; Saleh et al., 2002; Guglielmetti et al.,
92 2007; Grant et al., 2008; Guglielmetti et al., 2008; Santi et al., 2009). Moreover, effective and
93 theoretical values of vegetation parameters that are found in the literature are often limited to

94 agricultural crop data. These values are not consistent with each other, and difficult to compare
95 due to the variety of methods and procedures employed (Van de Griend and Wigneron, 2004).
96 As a result, there is a need to establish a direct physical link between the effective vegetation
97 parameterization and the theoretical description of absorption and scattering within the canopy.
98 This paper uses a first-order RT model and truck-based microwave measurements over natural
99 conifer stands to investigate this relationship by performing a physical analysis of the scattered
100 and emitted radiation from vegetated terrain. The microwave data used in this investigation were
101 collected over natural conifer stands located in Maryland in 2008 and 2009 (Kurum et al.,
102 submitted for publication). Physical measurements of the canopy and soil conditions were also
103 made.
104
105 Vegetation opacity of coniferous trees was obtained using three independent approaches that
106 provide effective, measured, and theoretical estimates. Results indicate that the effective optical
107 depth values are smaller than but of similar magnitude to both the theoretical and measured
108 values. The effective vegetation opacity was then set equal to the theoretical opacity in the zero-
109 order model, and an explicit expression for the effective albedo was obtained using the first-
110 order model. The resultant albedo was found to be comparable to the effective albedo
111 determined as a best-fit parameter that minimizes the difference between the microwave
112 observation and that value computed from the tau-omega model. The effective omega values
113 were less than half of the theoretical albedos [0.5 − 0.6 for tree canopies at L-band] (Ferrazolli et
114 al, 2002; Kurum et al., in press). This effective albedo implicitly accounts for multiple-scattering
115 effects by balancing the scattering darkening of albedo with the first-order scattering
116 contribution.

2 BASIC RADIATIVE TRANSFER MODELING OF VEGETATION

The commonly used approach to simulating the brightness temperature of vegetated terrain is to apply Radiative Transfer (RT) theory. The RT approach is a heuristic method based on the law of energy conservation that starts with the RT equation, which governs the transport of specific intensity through a random medium (Chandrasekhar, 1960). The theory assumes independent scattering and ignores coherent effects. The RT equation can be formulated for a continuous medium (Ishimaru, 1978; Fung, 1982; Wigneron et al, 1993) or a discrete medium (Tsang et al., 1985; Saatchi et al, 1994; Chauhan et al., 1994; Ferrazolli and Guerriero, 1996; Karam, 1997; Kurum et al., in press). The discrete modeling is more appropriate for a medium such as vegetation in which the individual scatterers have discrete configurations and have a dielectric constant that is distinct from the background (air). In the discrete approach, the vegetation layer is represented as an ensemble of scatterers. The scatterers are described by specified orientation, size, and position statistics. The layer is situated over a homogenous dielectric half-space representing the ground. The interface between the ground and canopy can be assumed to be rough. The different types of scatterers are usually assumed to be uniformly located within the vegetation layer, and to have canonical shapes. Leaves are modeled as dielectric disks (Le Vine et al., 1983; Le Vine et al., 1985). Branches and trunks are modeled as finite length dielectric cylinders of commensurate dimensions (Seker and Schneider, 1988; Karam et al., 1988). The single scattering characteristics of these constituents, when averaged, determine the attenuation and scattering properties of the canopy. The advantage of the discrete approach is that the results are expressed in terms of quantities (plant geometry and orientation statistics) that are related to the biophysical properties of individual plants.

RT theory can treat single and multiple-scattering in a medium consisting of random discrete scatterers. There are a number of approaches that can be used to calculate the multiple-scattering. This includes combining scattering contributions through exact numerical solutions (Tsang et al., 1985), a matrix doubling algorithm (Ferrazolli and Guerriero, 1996), and iterative methods (Tsang et al., 1985; Karam, 1997; Kurum et al., in press). An RT-based model in conjunction with the matrix-doubling algorithm was implemented by Ferrazzoli and Guerriero, 1996, and validated with various vegetation canopy data including forest. This model considers the multiple-scattering effects associated with the volume scattering and the interactions between multiple-layers in the vegetation canopy and the underlying ground surface. Karam, 1997, modeled the vegetation as a multi-layer random medium above a rough surface. This multi-layer model is based on an iterative solution of the RT equations using single scattering albedo as a perturbation (small) parameter. The model was validated with experimental data acquired over corn and soybean crops and also used to simulate emission from a walnut canopy. Alternatively, Peake's emissivity formula (Peake, 1959) in conjunction with a single scattering approximation (Lang, 1981), which is called Distorted Born Approximation (DBA), was implemented by Saatchi et al., 1994, and Chauhan et al., 1994 for a variety of land covers including grass and corn. Later, the same model was used to simulate emission from a forest canopy (Lang et al., 2001; Lang et al., 2006). Recently, Kurum et al., in press, developed a new microwave radiometry model that considers first-order scattering at L-band. The model was first validated against experimental data acquired over deciduous trees. It was then adapted to conifer trees which included a new representation of the forest floor (Kurum et al., submitted for publication). The model is based on an iterative solution of the RT equations by implementing the method of successive orders of scattering (Lenoble, 1985). The approach provides explicit expressions for

the zero- and first-order scattering and emission processes that occur within the canopy. The zero- and first-order RT solutions of this approach are summarized below.

2.1 Zero-Order Solution

The zero-order RT solution represents the solution to the non-scattering RT equations, where scattering is largely ignored by setting the scattering source functions to zero (Mo et al., 1982). This solution is also known as the tau-omega model. In this approximation, the vegetation canopy is treated as a bulk attenuating layer and scattering effects are introduced by means of a single-scattering albedo. The tau-omega model is given by

$$e_p^{(0)}(\theta) = \left[1 - \gamma_p^2(\theta) R_{gp}(\theta)\right] - \omega_p(\theta)\left[1 + \gamma_p(\theta) R_{gp}(\theta)\right]\left[1 - \gamma_p(\theta)\right] \quad (1.a)$$

where the ambient soil and vegetation temperatures are assumed approximately equal, the subscript p denotes vertical or horizontal polarization, i.e., $p = h$ or v. The first term represents the non-scattering case (independent of scattering albedo) and is also equivalent to the zero-order solution of the albedo expansion for canopies having uniform physical temperature profiles (Karam, 1997). The second term represents scattering darkening due to albedo. The combination of the first two terms represents the zero-order solution.

In (1.a), the quantity $\gamma_p(\theta)$ is the vegetation transmissivity, which is parameterized as

$$\gamma_p(\theta) = e^{-\tau_p \sec\theta} \quad (1.b)$$

where $\tau_p(\theta)$ is the vegetation opacity or optical thickness and is given by

$$\tau_p(\theta) = \kappa_{ep}(\theta) d \tag{1.c}$$

where θ is the observation angle from the nadir, d is thickness of the vegetation layer, and the volume extinction coefficient is defined by (Tsang et al., 1985):

$$\kappa_{ep}(\theta) = \frac{4\pi}{k_0} \sum_{\alpha} \rho_\alpha \Im m\left\{\langle f_{fpp}^{(\alpha)} \rangle\right\} \tag{1.d}$$

where $f_{fpp}^{(\alpha)}$ is the forward scattering amplitude of the α^{th} type of scatterer and each scatterer type α can be branch, leaf/needle, or trunk. The number density of each scatterer type α is denoted by ρ_α, and $k_0 = 2\pi/\lambda_0$ is the wave number where λ_0 is the free space wavelength. The sum is over all types of particles of which the vegetation is comprised. The angular brackets in this formula denote ensemble average over the angular and size statistics of particles. The tree site considered in this paper (refer to Section 3) is composed of natural Virginia pine (*Pinus virginiana*) trees. The pine needles are represented by average-size circular cylinders; hence, the averaging is done for orientation angles only. The trunks are vertical and for the stand studied here have a typical size. No averaging is therefore performed on trunks. The branch sizes are divided into several groups having an average length and diameter. An average orientation is then determined for each branch group.

An alternative empirical method widely used in the literature in determining the vegetation attenuation (Jackson and O'Neill, 1990; Jackson and Schmugge, 1991) is to relate the nadir optical depth to the vegetation water content (VWC) by

$$\tau_p(\theta = 0°) = b_p \times VWC \quad (1.e)$$

where b_p is an empirically determined constant based on vegetation type and polarization. Le Vine and Karam, 1996, have showed that for canopies whose structure (i.e. branches, trunks, etc.) are large compared to wavelength, the linear relation between attenuation and VWC does not hold and the b_p-parameter becomes a complex function of frequency, VWC, and architecture. As a result, this approach is more appropriate for agricultural crops at L-band.

In (1.a), the single scattering albedo is denoted by $\omega_p(\theta)$ and is given by (Tsang et al., 1985):

$$\omega_p(\theta) = \frac{\kappa_{sp}}{\kappa_{sp} + \kappa_{ap}} \quad (1.f)$$

where κ_{sp} is the scattering coefficient of the layer while κ_{ap} represents the total absorption coefficient. This is the albedo of the average scatterer in the canopy since the canopy is composed of more than one scatterer type. It represents the fractional power scattered from the average particle. In the case of a forest canopy, the scattering from large vegetation components such as branches and trunks is significant. The values of the composite albedos for both polarizations are generally in the range of 0.5 - 0.6 (Ferrazolli et al, 2002; Kurum et al., in press). This large albedo of a tree canopy leads to scatter-induced reduction in brightness temperature, and this scattering darkening effect for vegetation canopies (with large scatterers) should be balanced with a multiple-scattering contribution, which is missing in the tau-omega model.

Finally, $R_{gp}(\theta)$ is the microwave reflectivity of the forest floor. The ground under the tree canopy being considered here (refer to Section 3) was relatively smooth, where the surface *rms* height was on the order of 0.0–0.5 cm. Thus surface variation is rather low compared to the wavelength at L-band. As a result, only the coherent component of the surface roughness is important, and the diffuse component is ignored. It is also assumed that the rough surface under the forest follows Kirchhoff's approximation and has a Gaussian height distribution (Choudhury et al., 1979); therefore, the reflectivity of the rough surface is expressed as

$$R_{gp}(\theta) = \Gamma_{gp}(\theta) e^{-h\cos^2\theta} \tag{1.g}$$

where $\Gamma_{gp}(\theta)$ is the p-polarized Fresnel reflectivity of the average dielectric surface and the roughness height parameter is given by $h = 4\sigma^2 k_0^2$ in terms of surface rms height, σ and the wave number k_0.

In addition to roughness, for the study site used here, a moist organic litter layer needs to be considered. A litter layer can alter surface reflectivity significantly as verified by recent theoretical and experimental studies (Grant et al., 2007; Della Vecchia et al., 2007; Guglielmetti et al., 2008; Grant et al., 2009; Kurum et al., submitted for publication). In this paper, the ground reflectivity, $\Gamma_{gp}(\theta)$, is calculated using a recently developed three-layer soil model that includes a litter layer, an organic transition layer, and mineral soil (Kurum et al., submitted for publication). Ground observations collected approximately coincident with microwave measurements are utilized in this calculation.

2.2 First-Order Solution

The first-order solution of the RT equation with respect to the scattering source function is obtained by using the zero-order RT brightness temperature as an exciting source (Kurum et al., in press). This formulation adds a new scattering term to the tau-omega model. The improved model has an advantage over the conventional tau-omega model because the first-order solution accounts for scattering of the radiated emission from the ground and the vegetation layer. The first-order solution from the forest canopy leads to the following expression:

$$e_p^{(1)}(\theta) = e_p^{(0)}(\theta) + \Omega_p(\theta) \tag{2.a}$$

where the ambient temperatures of the vegetation layer and the ground are assumed to be the same, the polarization p can be horizontal (h) or vertical (v), and the quantity $e_p^{(0)}(\theta)$ is the zero-order solution given in (1.a). The parameter $\Omega_p(\theta)$ denotes the additional scattering contribution to the zero-order model. It represents the emission from the ground and the vegetation layer that is single- scattered from tree trunks, branches, and needles. The scattering component $\Omega_p(\theta)$ is composed of eight terms representing different scattering-mechanisms, which are given by:

$$\Omega_p(\theta) = \sum_j \left\{ \Omega_{jp}^{(s1)}(\theta) + \Omega_{jp}^{(sr1)}(\theta) \right\} \tag{2.b}$$

where the summation index $j \in \{G, U, D, DG\}$ denotes the scattering-mechanism types, i.e., the subscripts $G, U, D,$ and DG refer to the scattered radiation contributions due to ground emission, up-welling emission, down-welling emission, and down-welling emission followed by ground reflection, respectively. The scattered radiation from each mechanism arrives at the receiver either directly (denoted by $s1$) or through reflection from the ground (denoted by $sr1$). The pictorial illustration of the scattering processes and the explicit expressions for each scattering term are given in Kurum et al., in press.

3 MICROWAVE MEASUREMENTS OVER PINE TREES

The L-band microwave instrument system used in this study is called ComRAD for Combined Radar/Radiometer (O'Neill et al., 2006). The system is mounted on a 19-m hydraulic boom truck and has been developed jointly by NASA/GSFC and George Washington University. It includes a dual-pol 1.4 GHz radiometer and a quad-pol 1.25 GHz radar sharing the same 1.22-m parabolic dish antenna with 3-dB beamwidth of approximately 12º. The ComRAD's radiometer is a total power radiometer with a two-point internal calibration. The absolute accuracy and the sensitivity of the instrument are ±1 K and ±0.1 K, respectively. The truck radar system is configured around an Agilent E5071B ENA series vector network analyzer and operates in a stepped-frequency mode for all linear polarization combinations. External calibration of the radiometer is achieved using cold sky and ambient microwave absorber targets during each measurement run, while radar calibration is achieved using known microwave reflectors (flat disks and dihedral) at the beginning and end of each extended measurement series.

289 The ComRAD system was deployed to a coniferous tree site at NASA GSFC's Goddard
290 Geophysical and Astronomical Observatory (GGAO) campus in Greenbelt, Maryland, USA in
291 2008 and 2009 in order to provide active/passive measurements under controlled conditions. The
292 overall goal of the experiment was to improve our understanding of the microwave properties of
293 trees and their effect on SM retrieval algorithms. The passive dual-polarized microwave
294 measurements were acquired over a natural stand of Virginia pine trees at multiple incidence
295 angles (from 15º to 55º at 10º increments) with three different azimuth locations for each
296 incidence angle. Good dynamic range of ground moisture [a site-calibrated theta probe (TP)
297 readings varied 0.05 – 0.30 cm^3 cm^{-3}] under the pine trees was encountered during the entire
298 campaign. The site was divided into two equal plots of 60° sectors. This analysis focuses on
299 the data collected at one plot only (plot A). In addition to the regular observations, a separate
300 radar experiment with and without a trihedral corner reflector (1.22-m front edge length) under
301 trees of plot A was carried out on September 15, 2009 as shown in **Fig. 1**. The goal of this
302 experiment was to measure forest opacity directly by using changes in the radar backscatter as an
303 independent estimate. The data were collected at a 45º incidence angle only and at 19 different
304 azimuth locations (from 0º to 90º with 5º increments) to obtain an average.
305
306 The Virginia pine forest stand under investigation has an average height of 12-m, an average
307 basal area of 34 m^2 ha^{-1}, and an average diameter at breast height of 12.6 m. Virginia pine is a
308 medium sized evergreen conifer and is native to North America. The bark is thin, dark reddish-
309 brown and is broken into shallow plates. The short needles (4 cm to 8 cm) of Virginia pine range
310 from dark green to gray green to yellow-green and are usually twisted and in pairs. These trees
311 have a tendency to maintain a substructure of needleless branches (dead). The average leaf area

index (LAI) was measured 2.66 with a standard deviation of 0.16, which indicates a very homogeneous vegetation canopy. The forest floor has a distinct needle litter layer (undergone little or no decomposition) over an organic humus transition layer (partially and fully decomposed organic materials) lying on a well drained mineral soil. The average thickness of the litter layer was 0.8 cm. The organic humus layer thickness was 2.2 cm. The soils were loamy sand, with textures varying from 57% sand, 13.6% clay to 87% sand, 3.4% clay depending on location within the site. Surface roughness was very small, with an *rms* roughness height < 0.5 cm. More information on the ground and vegetation characteristics can be found in Kurum et al., submitted for publication.

4 ZERO-ORDER RADIATIVE TRANSFER PROPERTIES OF FOREST CANOPIES

Rigorous models with many input variables, such as the first-order RT model summarized in section 2, require a detailed knowledge of the vegetation and ground characteristics. These complex models are useful for understanding the sensitivity of the microwave sensor response to the forest canopy and underlying ground. On the other hand, simple models that require fewer parameters and *a priori* information, such as the tau-omega model, are necessary as they are to be implemented operationally in reliable inversion algorithms for sensors with a limited number of observations. There are a number of approaches that can be used to retrieve SM from low frequency passive microwave observations (Jackson, 1993; Owe et al., 2001; Njoku et al., 2003; Wigneron et al., 2007). Almost all of these are founded on the same zero-order RT solution (tau-omega model) due to its simplicity, ease of inversion and implementation, and its extensive validation over light to moderate vegetation.

Although it is not really suitable for forests, given the increased scatter from trees compared to grasses and crops, Ferrazzoli et al., 2002, proposed that the same zero-order approach might be applied to vegetation canopies with large scatterers, and that equivalent or effective parameters could be used. The basis of this approach lies in exploiting multi-angular and dual-polarization emissivity data in order to simultaneously retrieve geophysical products such as vegetation characteristics. The retrieved vegetation parameters are calibrated by means of a theoretical multiple-scattering model. Recently, this approach was tested using L-band microwave measurements over a coniferous (pine) and deciduous forest Grant et al., 2008.

The values of the effective vegetation optical depth $\overline{\tau}_e$ and single scattering albedo $\overline{\omega}_e$ are calculated by minimizing the following merit function:

$$\min \sqrt{\sum_{i=1}^{N} \sum_{p=h,v} \left[e_p^{(0)}(\overline{\tau}_e, \overline{\omega}_e, \theta_i) - e_{mp}(\theta_i) \right]^2} \qquad (3)$$

where $\overline{\tau}_e$ and $\overline{\omega}_e$ act as free parameters and are defined as independent of polarization and angle, θ_i is the observation angle from the nadir, N is the number of available incidence angles, e_{mp} is the measured p-polarized emissivity (the ratio of the measured brightness and the ambient temperatures), and $e_p^{(0)}$ is the modeled p-polarized zero-order RT solution given in (1.a). The subscript p denotes polarization [horizontal (h) or vertical (v)]. In this minimization, it is assumed that surface reflectivies are known *a priori*. The ground parameters collected approximately coincident with microwave measurements are utilized in conjunction with a three-layer dielectric forest floor model given in Kurum et al., submitted for publication.

356 The minimization procedure is applied to the multi-angular and dual-polarized microwave data
357 collected at the Virginia Pine forest site at different days (from August 1, 2008 to April 23,
358 2009). **Fig. 2** shows the plot of the measured emissivity data (collected on September 8, 2008)
359 over the observation angles from 15º to 55º along with the results of the fitted zero-order tau-
360 omega model. As seen from this example plot, the zero-order fit curve captures the angular and
361 polarization behavior of the data well. The polarization and angular dependence of the best-fit
362 zero-order emissivity stems from the polarization and angle discrimination in the surface
363 reflectivities only since the opacity and albedo values in (3) were assumed to be independent of
364 both polarization and angle of incidence. **Fig. 3** shows the retrieved vegetation opacities and
365 single scattering albedo values for each day. The average effective vegetation optical depths for
366 all measurements was 0.91 ± 0.10 and the average effective albedo value was 0.29 ± 0.10.
367 These results need to be evaluated in the context of their theoretical definitions in order to
368 provide a better understanding of these parameters in the retrieval algorithms over trees. Here,
369 the effective vegetation opacities will be compared against the results of two independent
370 approaches that provide optical depths, theoretical and measured. The theoretical technique is
371 based on the forward scattering theory and the measured on the radar corner reflector
372 observations. Following this analysis, an explicit expression for the effective albedo is then
373 obtained from the zero- and first- order RT model comparison.
374
375 **4.1 Opacity Comparison**
376 *4.1.1 Corner reflector approach:*
377 The forest opacity can also be measured directly by means of radar measurements with
378 trihedral corner reflectors. The corner reflectors are widely used for external radar

calibration since they yield large backscattering radar cross sections over wide azimuth and elevation angular ranges (Ulaby and Elachi, 1990). This approach is based on the expected strong return from a corner reflector under trees. It assumes that coupling between the corner reflector and the surrounding background and trees is small. Basically, the ratio between co-polarized radar backscatter measurements with the corner reflector under trees and in an open area provides the loss in propagation through trees. This retrieved forest opacity represents the measured opacity τ_{mp}, which is given by:

$$\tau_{mp} = -\frac{cos\,\theta}{2} ln \frac{\sigma^0_{ppmTC} - \sigma^0_{ppmT}}{\sigma^0_{ppmBC} - \sigma^0_{ppmB}} \quad (4.a)$$

where

$$\sigma^0_{ppmB} = \sigma^0_{ppb} \quad (4.b)$$

$$\sigma^0_{ppmBC} = \sigma^0_{ppb} + \sigma^0_{ppc} \quad (4.c)$$

$$\sigma^0_{ppmT} = \sigma^0_{ppd} + \sigma^0_{ppdr} \quad (4.d)$$

$$\sigma^0_{ppmTC} = \sigma^0_{ppd} + \sigma^0_{ppdr} + e^{-2\tau_{mp}\,sec\,\theta}\sigma^0_{ppc} \quad (4.e)$$

The quantity σ^0_{ppmT} is the measured backscattering coefficient from trees and it is composed of volume (σ^0_{ppd}) and double interaction terms [σ^0_{ppdr}] (Chauhan et al., 1991). The backscattering coefficient of the measurement with the trihedral corner reflector under trees

393 is denoted by σ^0_{ppmTC} and it includes a return from the corner reflector (σ^0_{ppc}) attenuated by
394 the vegetation volume ($e^{-2\tau_{mp}\,sec\,\theta}$). The radar measurement of the background in an open
395 field (σ^0_{ppb}) is represented by σ^0_{ppmB} and the measurement of the trihedral corner reflector in
396 an open area is denoted by σ^0_{ppmBC}.
397
398 **Fig. 4** shows the measured vegetation opacity values obtained at an angle of incidence of
399 45º using the radar returns with and without the trihedral corner reflector under the trees at
400 several azimuth locations. The pictures of the trihedral taken from front and behind during
401 the radar measured are given in **Fig. 1**. The data were collected at a 45º incidence angle only
402 and at 19 different azimuth locations (from 0º to 90º with 5º increments) to get an average
403 estimate. The measured vegetation optical depth at h-polarized channel is 1.33 ± 0.39 while
404 the v-polarized optical depth is 1.12 ± 0.38. Note that the outliers such as those when the
405 reflector was blocked by a tree, are discarded from the results.
406
407 *4.1.2 Theoretical approach*:
408 The vegetation propagation constant can also be determined by using the theoretical
409 definition given in (1.c) that involves the forward scattering amplitudes of each of the tree
410 constituents, averaged over all particle sizes and angle orientations. Since the forward
411 scattering amplitude of an arbitrary particle is a complex quantity, this medium will attenuate
412 the wave. This technique requires detailed measurements of size/angle distributions and
413 dielectric constants of the tree constituents (trunk, branches, and needles). The detailed
414 vegetation characteristics were obtained by destructive tree sampling; details are described in

415 Kurum et al., submitted for publication. The calculated forest parameters derived using this
416 technique represent theoretical values.
417
418 In **Fig. 5**, the angular and polarization dependences of the theoretical vegetation optical depth
419 are plotted. The figure also includes the measured h- and v-polarized average vegetation
420 opacity at an incidence angle of 45º and the polarization independent average effective
421 opacity obtained through minimization of (3), for comparison purposes. Based on these
422 plots, the followings can be concluded:
423 a) The theoretical opacity depends weakly on angle and polarization. This can be
424 attributed to the horizontal orientation of primary branches that are the main source of
425 scattering and extinction. This result provides a basis to choosing to use effective
426 values that are independent of polarization and angle in (3) for conifer trees, which
427 are generally made of horizontal branches.
428 b) The measured opacities are higher than the other results, and more polarization
429 dependent than the theoretical result at an incidence angle of 45º. This discrepancy
430 could be attributed to the assumption to ignore the coupling between the corner
431 reflector, the surrounding background, and trees in the radar technique, and the
432 assumption of the uniform spatial distribution of the different types of scatterers
433 within the vegetation layer in the vegetation scattering model.
434 c) The effective values are smaller than but of similar magnitude to both the measured
435 and theoretical values. This implies that the opacity values retrieved by the tau-omega
436 model could be approximated by the theoretical values and it also preserves the
437 physical meaning.

438 **4.2 Albedo Comparison**

439

440 As previously mentioned, the scattering from large vegetation components such as branches
441 and trunks is significant. The values of the composite albedos for both polarizations are
442 generally in range of 0.5 - 0.6. This large albedo of a tree canopy leads to scatter-induced
443 reduction in brightness temperature, and this scattering darkening effect should be balanced
444 with a multiple-scattering contribution, which is missing in (1). The first-order RT solution
445 is sufficient for describing emission and scattering processes within the forest canopy at L-
446 band (Kurum et al., in press). Under the assumption that effective vegetation opacity in the
447 tau-omega model is the same as the theoretical opacity for tree canopies (given the increased
448 scatter from trees compared to grasses and crops), one can relate the zero-order solution
449 given in (1.a) with an effective scattering albedo to the first-order solution given in (2.a) with
450 the theoretical albedo i.e.,

451
452
$$e_p^{(0)}\left(\overline{\omega}_{ep}, \gamma_p, R_{gp}\right) = e_p^{(1)}\left(\omega_p, \gamma_p, R_{gp}\right) \tag{5}$$

453
454
455 Upon solving eq. (5) for the effective scattering albedo yields:

456

$$\overline{\omega}_{ep}(\theta) = \omega_p(\theta) - \frac{\Omega_p(\theta)}{\left[1 + \gamma_p(\theta) R_{gp}(\theta)\right]\left[1 - \gamma_p(\theta)\right]} \tag{6}$$

457
458

459 Due to the last term in (6), the effective single scattering albedo, $\overline{\omega}_{ep}(\theta)$, depends on all the
460 processes taking place within the canopy and ground. In (6), the theoretical albedo, $\omega_p(\theta)$,
461 and vegetation transmissivity, $\gamma_p(\theta)$, are calculated using the canopy parameters derived by

462 destructive sampling in the scattering model. The ground reflectivity, $R_{gp}(\theta)$, is calculated
463 by the three-layer soil model, where the ground observations collected approximately
464 coincident with microwave measurements are utilized. Calculation of the first-order
465 scattering term, $\Omega_p(\theta)$, requires both vegetation and ground parameters.
466
467 **Fig. 6** shows results from both the theoretical albedo given in (1.f) and the simulated
468 effective albedo given in (6) for the conifer forest as a function of incidence angle for both
469 polarizations. As seen from the plot, the theoretical scattering albedo is around 0.6 for both
470 polarizations and depends weakly on angle of incidence and polarization because of the
471 horizontal orientation of the primary branches. The simulated effective albedo values are in
472 the range of 0.2 - 0.3, which are less than half of the theoretical ones and are higher than the
473 SMOS default albedo value of 0.1 for forest canopies (Grant et al., 2008). This reduced
474 albedo accounts for multiple-scattering effects by balancing the scattering darkening of
475 albedo with the first-order scattering contribution as seen from the last term in (6). The plot
476 also indicates that effective albedo values decrease monotonically with increasing angle.
477 This is due to the increase in the contribution of the first-order scattering with increasing
478 angle (Kurum et al., in press).
479
480 **Fig. 7** shows the effect of ground moisture on the effective single scattering albedo. In the
481 plot, the effective albedo values of (3) are obtained from measured data as a best-fit
482 parameter that minimizes the difference between measured data and the zero-order RT model
483 results for all available incidence angles while the simulated albedos are calculated from (6)
484 at incidence angles of 15° and 45°. In the calculation of the best-fit effective albedo,

485 vegetation parameters are taken to be independent of polarization and angle while horizontal
486 (solid lines) and vertical (dashed lines) polarizations are considered in the simulations. The
487 results represent the albedo values over a wide range of ground conditions, where ground
488 moisture varied between 0.05–0.30 cm^3 cm^{-3}. The simulation results indicate a slight
489 increase in the effective albedo with the increase in ground moisture. On the other hand, the
490 measured values seem to be independent of the moisture content of the ground but have a
491 magnitude similar to the simulated ones. It can be concluded that the retrieved effective
492 albedo is different from the theoretical definition and it is not the albedo of single forest
493 elements anymore. It is now a global parameter, which depends on all the processes taking
494 place within the canopy, including multiple-scattering.
495
496 ## 5 CONCLUSION AND SUMMARY
497
498 Inversion of the tau-omega model requires effective or equivalent values for the whole canopy.
499 There is a need to establish a direct physical link between these effective vegetation parameters
500 and their formal definitions. This paper used a first-order RT model and truck-based microwave
501 measurements over a natural conifer stand to investigate this relationship. Physical analysis of
502 the scattered and emitted radiation from vegetated terrain were performed using microwave data
503 collected over a natural conifer stand located in Maryland in 2008 and 2009.
504
505 Vegetation opacity of coniferous trees was obtained using three independent approaches that
506 provide effective, measured, and theoretical estimates. The effective values were found to be
507 smaller than but of similar magnitude to both measured and theoretical values. This implies that

508 the opacity values retrieved by the tau-omega model could be approximated by the theoretical
509 values while preserving their physical meaning. An explicit expression was provided for the
510 effective albedo by relating the zero-order model to the first-order model with an effective
511 scattering albedo after setting the vegetation opacity of the zero-order approach equal to the
512 theoretical opacity. This expression accounts for all the processes taking place within the canopy
513 including multiple-scattering and ground reflection. The effective albedo was also determined as
514 a best-fit parameter that minimizes the difference between microwave observation and the
515 parametric model. The resulting simulated and measured effective albedos were found similar
516 magnitude but less than half of those estimated using the theoretical definition. This reduced
517 albedo implicitly accounts for multiple-scattering effects by balancing the scattering darkening
518 of albedo with the first-order scattering contribution. The retrieved effective albedo is different
519 from theoretical definitions and not the albedo of single forest elements anymore, but it becomes
520 a global parameter, which depends on all the processes taking place within the canopy, including
521 multiple-scattering.

6 REFERENCES

Chandrasekhar S. (1960). *Radiative Transfer*. New York, NY: Dover Publications Inc.

Chauhan N. S., Lang R. H., & Ranson K. J. (1991). Radar modeling of a boreal forest. *IEEE Transaction on Geosciences and Remote Sensing,* 29 (4), 627-638.

Chauhan N., LeVine D. M., & Lang R. H. (1994). Use of discrete scatter model to predict active and passive microwave sensor response to corn: Comparison of theory and data., *IEEE Transactions on Geoscience and Remote Sensing*, 32 (2), 416–426.

Choudhury B. J., Schmugge T. J., Newton R. W., & Chang A. (1979). Effect of surface roughness on the microwave emission from soils. *J. Geophys. Res*., 84 (C9), 5699–5706.

Della Vecchia, A., Saleh, K., Ferrazzoli, P., Guerriero, L., and Wigneron, J. P. (2006). Simulating L-band emission of coniferous forests using a discrete model and a detailed geometrical representation. *IEEE Geoscience and Remote Sensing Letters*, 3 (3), 364-368.

Della Vecchia A., Ferrazzoli P., Wigneron J. P., & Grant J. P. (2007). Modeling forest emissivity at L-band and a comparison with multitemporal measurements. *IEEE Geoscience and Remote Sensing Letters*, 4 (4), 508– 512.

544 Entekhabi D., Asrar G. R., Betts, A. K., Beven, K. J., Bras, R. L., Duffy, C. J., Dunne, T.,
545 Koster, R. D., Lettenmaier, D. P., Mclaughlin, D. B., Shuttleworth, W. J., Van Genuchten,
546 M. T., Wei M.Y. & Wood, E. F. (1999) . An agenda for land-surface hydrology research and
547 a call for the second international hydrological decade. *Bulletin of the American*
548 *Meteorological Society*, 80 (10), 2043-2057.
549
550 Entekhabi D., Njoku E., O'Neill P. E., Kellogg K., Crow W., Edelstein W., Entin J., Goodman
551 S., Jackson T. J., Johnson J., Kimball J., Piepmeier J., Koster R., Martin N., McDonald K.,
552 Moghaddam M., Moran S., Reichle R., Shi J.C., Spencer M., Thrman S., Tsang L., & Jakob
553 V. (2010) .The Soil Moisture Active and Passive (SMAP) Mission. *Proceedings of the IEEE*,
554 98 (5), 704 - 716.
555
556 Ferrazzoli P. & Guerriero L. (1996). Passive microwave remote sensing of forests: A model
557 investigation," *IEEE Transactions on Geoscience and Remote Sensing*, 34 (2), 433–443.
558
559 Ferrazolli P., Guerriero L., & Wigneron J. P. (2002). Simulating L-band emission of forests in
560 view of future satellite applications. *IEEE Transactions on Geoscience and Remote Sensing*,
561 40 (12), 2700-2708.
562
563 Fung A. K. (1982). A review of volume scatter theories for modeling applications. *Radio*
564 *Science*, 17 (5), 1007-1017.
565

566 Grant J. P., Wigneron J. P., Van de Griend A. A., Kruszewski A., Schmidl S. S., & Skou N.
567 (2007). A field experiment on microwave forest radiometry: L-band signal behavior for
568 varying conditions of surface wetness. *Remote Sensing of Environment*, 109 (1), 10–19.
569
570 Grant J. P., Saleh K. C., Wigneron J. P., Guglielmetti M., Kerr Y. H., Schwank M., Skou N., van
571 de Griend A. A. (2008). Calibration of the L-MEB Model Over a Coniferous and a
572 Deciduous Forest," *IEEE Transactions on Geoscience and Remote Sensing*, 46 (3), 808-818.
573
574 Grant J. P., Van de Griend A. A., Schwank M., & Wigneron J. P. (2009). Observations and
575 modeling of a pine forest floor at L-band. *IEEE Transaction on Geoscience and Remote*
576 *Sensing*, 47 (7), 2024–2034.
577
578 Guglielmetti M., Schwank M., Matzler C., Oberdorster C., Vanderborght J., & Fluhler H. (2007).
579 Measured microwave radiative transfer properties of a deciduous forest canopy," *Remote*
580 *Sensing of Environment*, 109 (4), 523–532.
581
582 Guglielmetti M., Schwank M., Mätzler C., Oberdorster C., Vanderborght J., & Fluhler H. (2008).
583 FOSMEX: Forest Soil Moisture Experiments with microwave radiometry. *IEEE Transaction*
584 *on Geoscience and Remote Sensing*, 46 (3), 727–735.
585
586 Ishimaru A. (1978). *Wave Propagation and Scattering in Random Media, Part IV: Waves in*
587 *random continuum and turbulence*. (vol. 2). New York: Academic Press.
588

589 Jackson T. J. & O'Neill P. E. (1990). Attenuation of soil microwave emissivity by corn and
590 soybeans at 1.4 and 5 GHz. *IEEE Transactions on Geoscience and Remote Sensing*, 28 (5),
591 978-980.
592
593 Jackson T. J. & Schmugge, T. J. (1991). Vegetation effects on the microwave emission of soils.
594 *Remote Sensing of Environment*, 36 (3), 203-212.
595
596 Jackson T. J. (1993). Measuring surface soil moisture using passive microwave remote sensing.
597 *Hydrological Processes*, 7, 139-152.
598
599 Jackson T. J., Le Vine D. M., Hsu A. Y., Oldak A., Starks P. J., Swift C. T., Isham J. D., &
600 Haken M. (1999). Soil moisture mapping at regional scales using microwave radiometry: the
601 Southern Great Plains hydrology experiment. *IEEE Trans. on Geoscience and Remote*
602 *Sensing*, 37 (5), 2136-2151.
603
604 Kerr Y. H., Waldteufel P., Wigneron J. P., Delwart S., Cabot F., Boutin J., Escorihuela M. J.,
605 Font J., Reul N., Gruhier C., Juglea S. E., Drinkwater M. R., Hahne A., Martin-Neira M., &
606 Mecklenburg S. (2010). The SMOS Mission: New Tool for Monitoring Key Elements of the
607 Global Water Cycle. *Proceedings of the IEEE*, 98 (5), 666 - 687.
608
609 Karam M. A., Fung A., & Antar Y. (1988). Electromagnetic wave scattering from some
610 vegetation samples. *IEEE Transactions on Geoscience and Remote Sensing*, 26 (6), 799–808.
611

612 Karam M. A. (1997). A physical model for microwave radiometry of vegetation. *IEEE*
613 *Transactions on Geoscience and Remote Sensing*, 35 (4), 1045– 1058.
614
615 Kurum M., Lang R. H., O'Neill P. E., Joseph A. T., Jackson T. J., & Cosh M. (in press). A First-
616 Order Radiative Transfer Model for Microwave Radiometry of Forest Canopies at L-band.
617 *IEEE Transaction on Geoscience and Remote Sensing*.
618
619 Kurum M., O'Neill P. E., Lang R. H., Cosh M., Joseph A. T., & Jackson T. J. (submitted for
620 publication). Impact of Conifer Forest Litter on Microwave Emission at L-band. *IEEE*
621 *Transaction on Geoscience and Remote Sensing*.
622
623 Lang R. H. (1981). Electromagnetic backscattering from a random distribution of lossy dielectric
624 scatterers. *Radio Sci.,* 16 (1), 15–30.
625
626 Lang R. H., Utku C., de Matthaeis P., Chauhan N., & LeVine D. M. (2001). ESTAR and model
627 brightness temperatures over forests: Effects of soil moisture. *In Proc. IEEE IGARSS*, 3,
628 1300–1302.
629
630 Lang R. H., Chauhan N., Utku C., & Le Vine D. M. (2006). L-Band Active and Passive Sensing
631 of Soil Moisture through Forests. I*n Proc. IEEE MicroRad*, 193 – 196.
632

633 LeVine D. M., Meneghini R., Lang R. H., & Seker S. S. (1983). Scattering from arbitrarily
634 oriented dielectric disks in the physical optics regime. *J. Opt. Soc. Amer.,* 73 (10), 1255–
635 1262.
636
637 LeVine D. M., Schneider A., Lang R. H., & Carter H. G. (1985). Scattering from thin dielectric
638 disks," *IEEE Trans. Antennas Propag*., AP-33 (12), 1410–1413.
639
640 Le Vine D. M. and Karam M. A. (1996). Dependence of attenuation in a vegetation canopy on
641 frequency and plant water content. *IEEE Transactions on Geoscience and Remote Sensing*,
642 34 (5), 1090–1096.
643 Lenoble J., (Editor). (1985), *Radiative Transfer in Scattering and Absorbing Atmospheres:*
644 *Standard Computational Procedures*. Hampton, VA: A. Deepak.
645
646 Mo T., Choudhury B., Schmugge T., Wang J., & Jackson T. A. (1982). Model for Microwave
647 Emission from Vegetation Covered Fields. *Journal of Geophysical Research*, 87(C13),
648 11229-11238.
649
650 Njoku E., Jackson E., Lakshmi V., Chan T., & Nghiem S. (2003). Soil Moisture Retrieval from
651 AMSR-E. *IEEE Transactions on Geoscience and Remote Sensing*, 41 (2), 215-229.
652
653 O'Neill P. E., Lang R. H., Kurum M., Carver K. R., & Utku C. (2006). Multi-sensor microwave
654 remote sensing of NASA's Combined Radar/Radiometer (ComRAD) system. *In Proc. IEEE*
655 *MicroRad*, San Juan, Puerto Rico, 50–54.

Owe M., de Jeu R., & Walker J. (2001). A methodology for surface soil moisture and vegetation optical depth retrieval using the microwave polarization difference index. *IEEE Trans. Geosci. Rem. Sens*., 39 (8), 1643-1654.

Peake W. (1959). Interaction of electromagnetic waves with some natural surfaces. *IRE Trans. Antennas Propag*. 7 (5), 324–329.

Saatchi S. S., Le Vine D. M., & Lang R. H. (1994). Microwave backscatter and emission model for grass canopies. *IEEE Transactions on Geoscience and Remote Sensing*, 32 (1), 177–186.

Saleh K., Wigneron J.P., Calvet J.C., & López-Baeza E. (2002). Modeling of L-band brightness temperature over land from STARRS data. I*n Proc. of First Results Workshop on EuroSTARRS, WISE, LOSAC Campaigns*, Toulouse (France).

Santi E., Paloscia S., Pampaloni P., & Pettinato S. (2009). Ground-based microwave investigations of forest plots in Italy. *IEEE Trans. on Geoscience and Remote Sensing,* 47 (9), 3016–3025.

Seker S. S. & Schneider A. (1988). Electromagnetic scattering from a dielectric cylinder of finite length. *IEEE Trans. Antennas Propag*., 36 (2), 303–307.

678 Tsang L., Kong J. A., & Shin R. T. (1985). *Theory of Microwave Remote Sensing*. New York:
679 John Wiley & Sons, (Chapter 3).
680
681 Ulaby F. T. (Editor, Preface) & Elachi C. (Preface). (1990). *Radar Polarimetry for Geoscience*
682 *Applications*. Artech House Publishers, (Chapter 5).
683
684 Wigneron J. P., Calvet J. C., Kerr Y. H., Chanzy A., & Lopes A. (1993). Microwave emission of
685 vegetation: Sensitivity to leaf characteristics. *IEEE Transactions on Geoscience and Remote*
686 *Sensing*, 31, 716–726.
687
688 Wigneron J. P., Chanzy A., Calvet J. C., & Bruguier N. (1995). A simple algorithm to retrieve
689 soil moisture and vegetation biomass using passive microwave measurements over crop
690 fields. *Remote Sensing of Environment*, 51 (3), 331−341.
691
692 Wigneron J. P., Kerr Y. H., Waldteufel P., Saleh K., Escorihuela M.-J., Richaume P., Ferrazzoli
693 P., de Rosnay P., Gurney R., Calvet J. C., Grant J. P., Guglielmetti M., Hornbuckle B.,
694 Matzler C., Pellarin T., & Schwank M. (2007). L-band microwave emission of the biosphere
695 (L-MEB) model: Description and calibration against experimental data sets over crop fields.
696 *Remote Sensing of Environment*, 107, 639-655.
697
698 Van de Griend A. A. & Wigneron J. P. (2004). On the measurement of microwave vegetation
699 properties: some guidelines for a protocol. *IEEE Transactions on Geoscience and Remote*
700 *Sensing*, 42 (10), 2277-2289.

List of Figures

Fig. 1. Pictures of the trihedral taken from (a) front and (b) behind during the radar measurements.

Fig. 2. Radiometer angular response from Virginia pine forest and the fitted zero order model for data collected on September 08, 2008.

Fig. 3. Effective vegetation optical thicknesses and single scattering albedos from the multi-angular emissivity data.

Fig. 4. Measured vegetation optical thicknesses from trihedral experiment at incidence angle of 45º on September 15, 2009.

Fig. 5. Theoretical vegetation optical thicknesses are plotted as function incidence angle and compared with effective and measured values.

Fig. 6. The theoretical single scattering albedo in eq. (1.f) and simulated effective albedo in eq. (6) of Virginia pine trees are plotted as a function of incidence angle.

Fig. 7. The simulated [using (6)] and measured [using (3)] effective albedos of Virginia pine trees are plotted as a function of ground moisture (TP readings).

(a)

(b)

Fig. 1. Pictures of the trihedral taken from (a) front and (b) behind during the radar measurements.

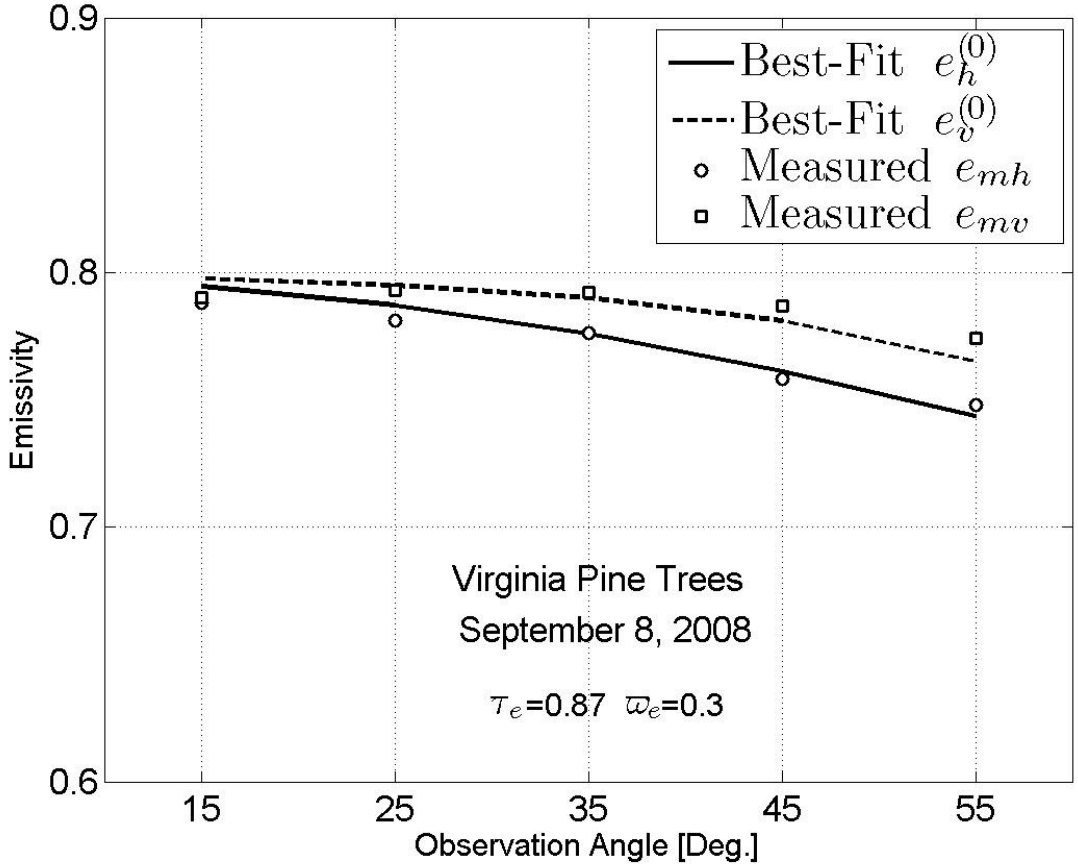

729

730 **Fig. 2.** Radiometer angular response from Virginia pine forest and the fitted zero order model for

731 data collected on September 08, 2008.

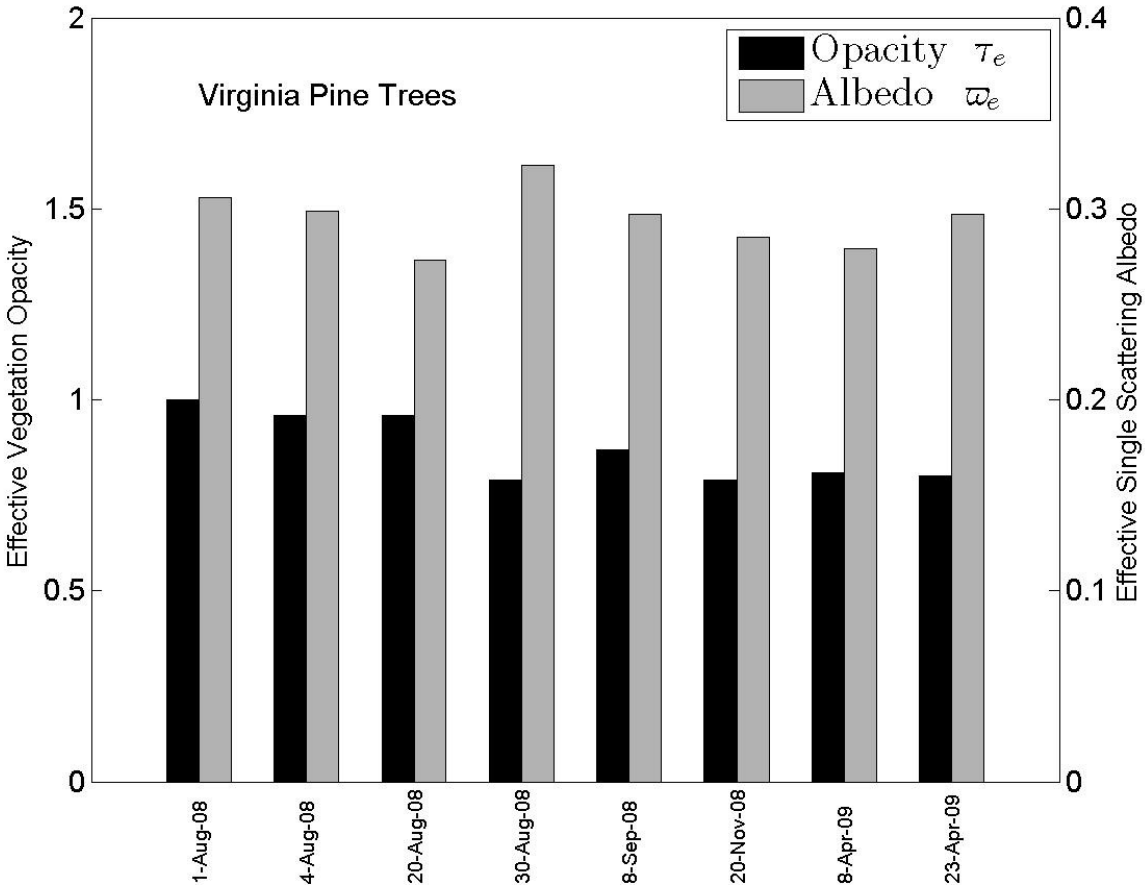

732

733 **Fig. 3.** Effective vegetation optical thicknesses and single scattering albedos from the multi-

734 angular emissivity data.

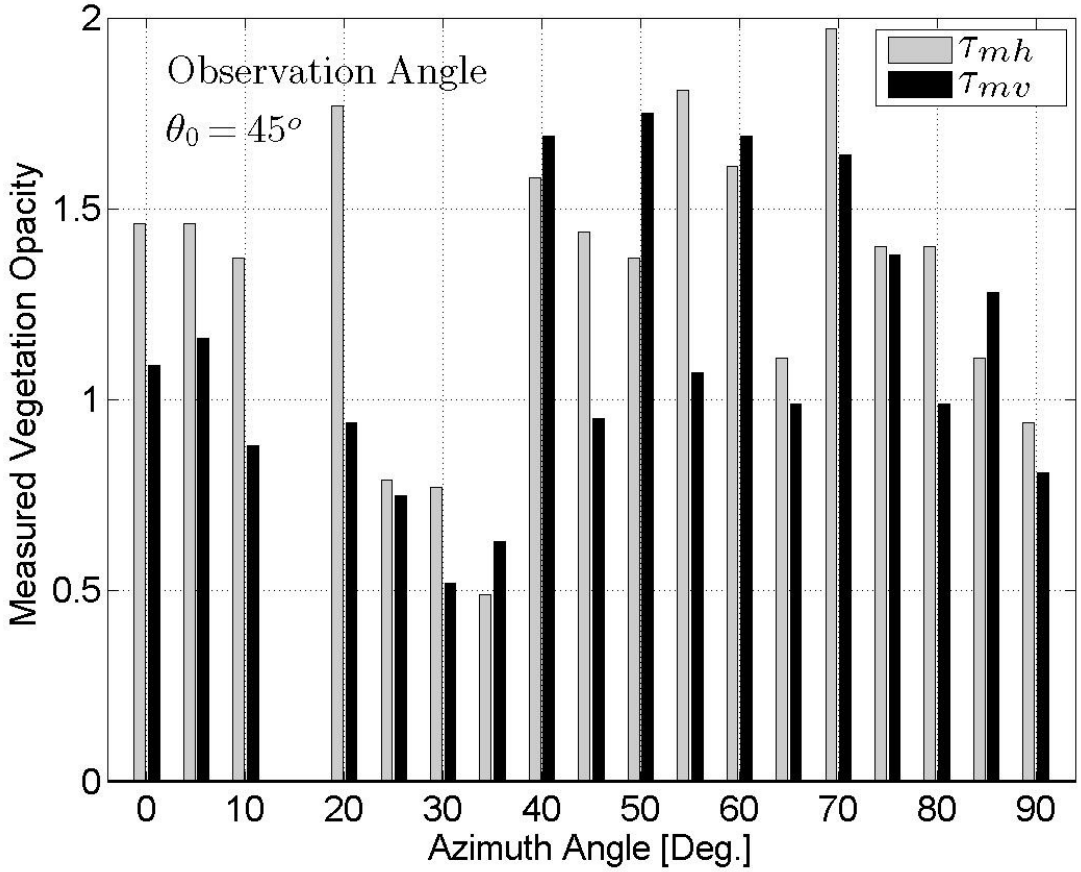

735

736 **Fig. 4.** Measured vegetation optical thicknesses from the trihedral experiment at incidence angle

737 of 45º on September 15, 2009.

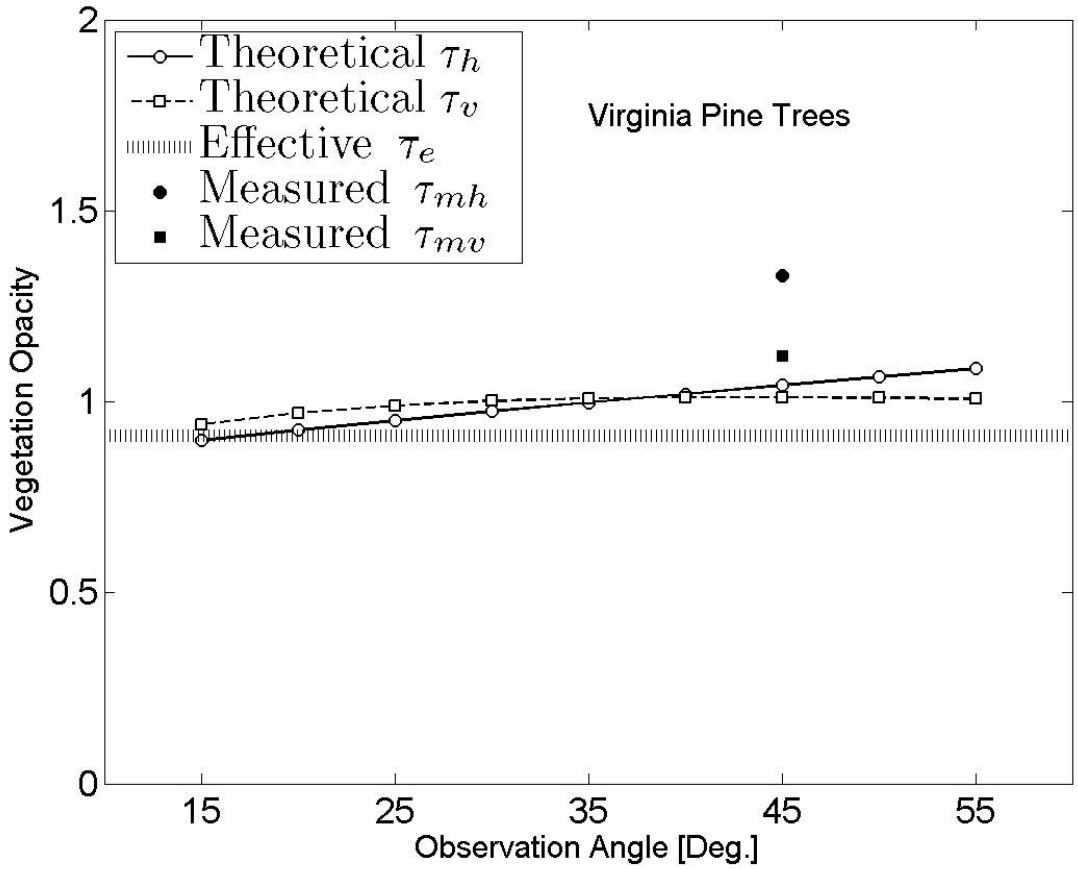

738

739 **Fig. 5.** Theoretical vegetation optical thicknesses are plotted as function incidence angle and

740 compared with effective and measured values.

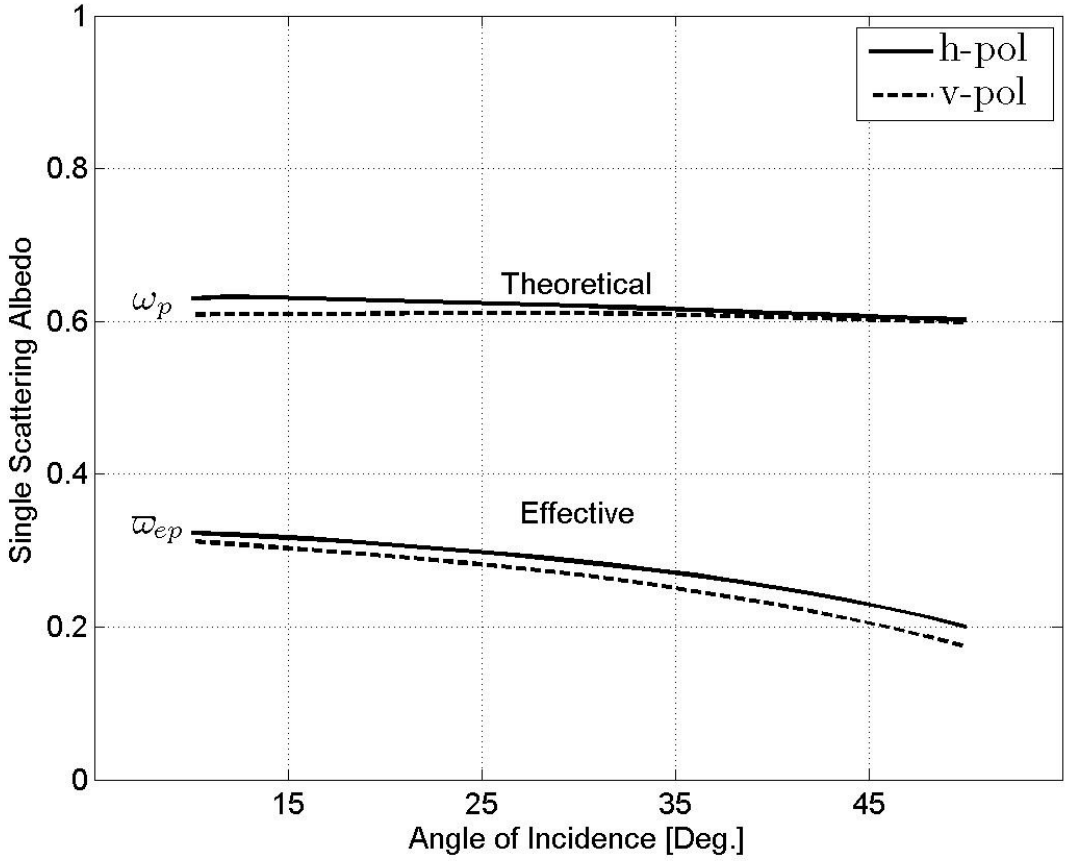

741

742 **Fig. 6.** The theoretical single scattering albedo in eq. (1.f) and simulated effective albedo in eq.

743 (6) of Virginia pine trees are plotted as a function of incidence angle.

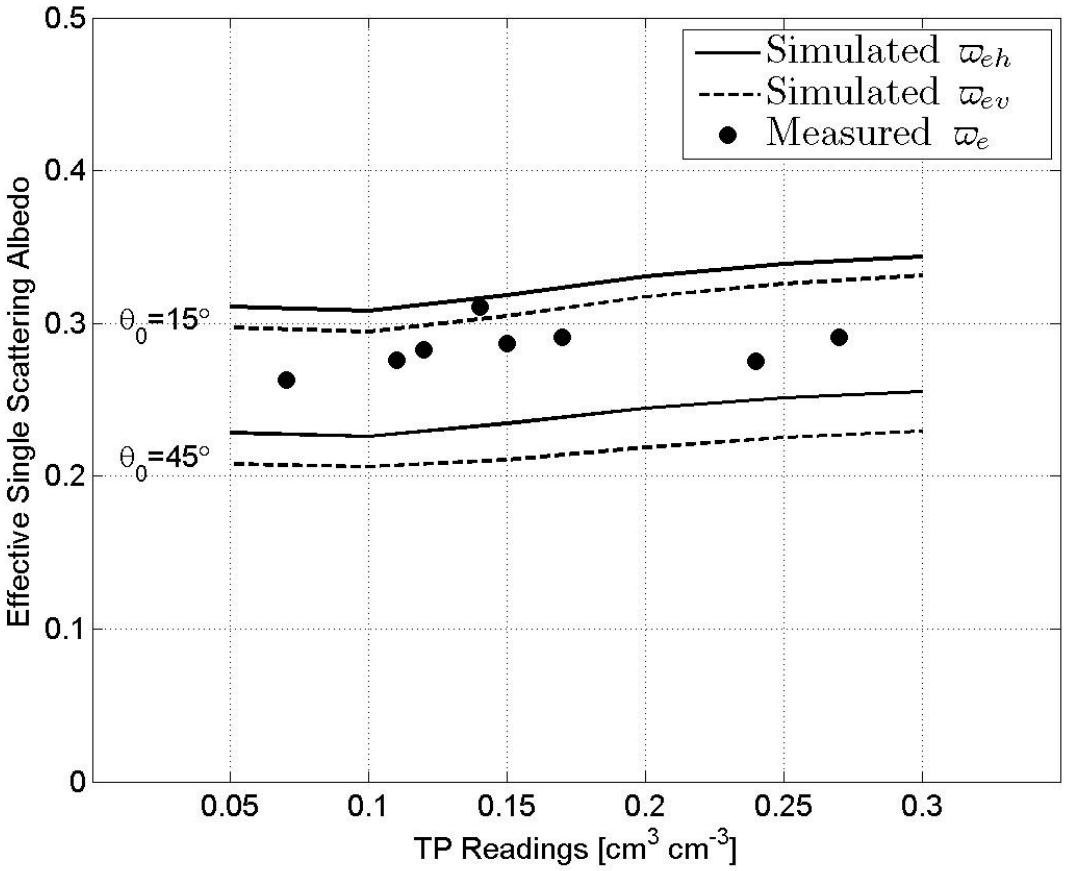

744

745 **Fig. 7.** The simulated [using (6)] and measured [using (3)] effective albedos of Virginia pine

746 trees are plotted as a function of ground moisture (TP readings).